Plasma Chemistry and Plasma Processing (2023) 43:513–532
https://doi.org/10.1007/s11090-022-10308-5

ORIGINAL PAPER

Investigation of Partial Oxidation of Methane in a Cold Plasma Reactor with Detailed Product Analysis

Silvie Müller[1] · Eckhard Ströfer[1] · Maximilian Kohns[1] · Kerstin Münnemann[1] · Erik von Harbou[2] · Hans Hasse[1]

Received: 29 August 2022 / Accepted: 28 November 2022 / Published online: 21 December 2022
© The Author(s) 2022

Abstract

Cold plasma is a partially ionized state of matter that unites high reactivity and mild conditions. Therefore, cold plasma reactors are intriguing for reaction engineering. In this work, a laboratory scale dielectric barrier discharge (DBD) cold plasma reactor was designed, set up, and used for studying the influence of the specific energy input (*SEI*) on the product spectrum of the partial oxidation of methane. In total, 23 experiments were carried out near ambient conditions with a molar reactant ratio of methane to oxygen of 2:1 at *SEI* between 0.3 and 6.0 J cm^{-3}. The feed also contained argon at a mole fraction of 0.75 mol mol^{-1}. The product stream was split into a fraction that was condensed in a cold trap and the remaining gaseous fraction. The latter was analyzed at-line in a gas chromatograph equipped with a dual column and two carrier gases. The condensed fraction was analyzed by qualitative and quantitative ^{1}H and ^{13}C NMR spectroscopy, Karl Fischer titration, and sodium sulfite titration. In the product stream, 16 components were identified and quantified: acetic acid, acetone, carbon dioxide, carbon monoxide, ethanol, ethane, ethene, ethylene glycol, formaldehyde, formic acid, hydrogen, methanol, methyl acetate, methyl hydroperoxide, methyl formate, and water. A univariant influence of the *SEI* on the conversions of methane and oxygen and the selectivities to the products was observed. The experimental results provided here are an asset for developing reaction kinetic models of the partial oxidation of methane in DBD plasma reactors.

Keywords DBD · Cold plasma reactor · Specific energy input · Partial oxidation of methane · NMR

✉ Hans Hasse
hans.hasse@mv.uni-kl.de

[1] Laboratory of Engineering Thermodynamics, TU Kaiserslautern, Erwin-Schrödinger-Str. 44, 67663 Kaiserslautern, Germany

[2] Laboratory of Reaction and Fluid Process Engineering, TU Kaiserslautern, Erwin-Schrödinger-Str. 44, 67663 Kaiserslautern, Germany

Introduction

Cold plasma technology is interesting as the presence of excited species, radicals, ions, and free electrons in the plasma opens up new reaction pathways at mild conditions [1]. Dielectric barrier discharge (DBD) cold plasma technology is particularly suited for applications in reaction engineering: it is comparatively easy to operate and also works at ambient conditions [2, 3] and it has a large volume excitation in an energy range capable for the excitation of atomic and molecular species and the breaking of chemical bonds to initiate chemical reactions [4, 5]. The most important application of DBD cold plasma is the generation of ozone, first described by Siemens [6]. Today, there is a growing number of possible applications that are discussed, such as wastewater treatment [7], decomposition of volatile organic compounds [8], and the synthesis of value-added products in organic chemistry [5, 9–15]. For the latter, the DBD cold plasma is often investigated in the context of C_1 chemistry, namely for the partial oxidation of methane (CH_4) with oxygen (O_2) [10, 16–41]. Many of those investigations also combine the DBD cold plasma with a catalyst [21, 22, 27–29]. In some of these studies, also other educts, which undergo reactions, such as water [10, 24, 30, 31], hydrogen [32], and starch [33] were added. By adding noble gases to the feed, such as helium or argon, explosion limits can be circumvented [42], the discharge uniformity is improved, and the breakdown voltage is decreased [43, 44]. Most of these studies were carried out with a focus on chemistry in the plasma and not with a focus on reaction engineering aspects. With the present work, we want to contribute to closing this gap. For this reason, we focus on the basic reaction system of the uncatalyzed partial oxidation of CH_4 with pure O_2 in the presence of the inert gas argon (Ar).

Investigations of cold plasma reaction technology are challenging not only because it requires applying high voltage, but in particular because a plethora of different components are formed which need to be analyzed, both qualitatively and quantitatively. In the literature, the analysis of the product stream from cold plasma oxidation of CH_4 with O_2 usually focuses on the synthesis gas components hydrogen and carbon monoxide as well as on a few oxygen-containing compounds, such as methanol or formaldehyde. The most comprehensive studies of cold plasma oxidation of CH_4 have been carried out by Larkin et al. [20], Goujard et al. [25], and Chawdhury et al. [27], but even in these, quantitative data on products such as acetic acid, ethanol, and methyl formate are often only available for a single experiment. Astonishingly, an important product does not seem to have been analyzed quantitatively in the literature studies so far: water.

In the present work, the product stream from the reactor was split into a fraction that was condensed in a cold trap and the remaining gaseous fraction. The gaseous fraction of the product stream was analyzed at-line in a gas chromatograph (GC) with a thermal conductivity detector. The use of a double column and two different carrier gases allowed for the analysis of a variety of components, including: CH_4, O_2, Ar, carbon monoxide, carbon dioxide, ethane, ethene, and hydrogen. The fraction from the cold trap containing components such as alcohols, acids, water, and formaldehyde was analyzed offline. The main tool applied for this analysis was quantitative nuclear magnetic resonance (NMR) spectroscopy, which was complemented by titration techniques (Karl Fischer for water and sodium sulfite for formaldehyde). The analytical procedures were based on previous experience of our group with similar systems [45–50].

With this experimental and analytical set-up, we conducted a series of 23 experiments, in which the reactor was always operated at ambient pressure and near-ambient temperature in steady-state. The goal of these experiments was to elucidate the influence of the

specific energy input *SEI*, i.e., electrical power divided by volumetric feed flow rate, on the spectrum of the product stream. The molar reactant ratio of (CH_4:O_2) and the molar dilution ratio of (reactants:Ar) were kept constant in all experiments. The new results extend the knowledge on the influence of the *SEI* on the conversions and selectivities in cold plasma partial oxidation of CH_4 with O_2 considerably.

Materials and Methods

Experiments

Figure 1 shows the cold plasma reactor; Fig. 2 shows the set-up for analyzing the product stream. The cold plasma reactor consists basically of a tube (inner diameter 12 mm), in which the high voltage electrode is mounted concentrically in a second tube (outer diameter 6 mm). The entire reactor has a length of 350 mm. It is made from borosilicate glass and surrounded by a thermostatization jacket, through which water was circulated, and which contained the ground electrode. The active volume of the reactor in the zone, where plasma can be generated, is about 26.3 cm^3. Both electrodes were made from 1.4571 stainless steel (X6CrNiMoTi17-12-2). They were connected to a high voltage generator from GBS Elektronik (MINIPULS Universal). The primary voltage supply of the MINIPULS Universal was adjustable in a range from 0 to 60 V with a frequency from 0.5 to 50 kHz. The output signal of the MINIPULS Universal is a sinusoidal, high frequency high voltage $u(t)$, where t is the time, and the maximal effective output power is 700 W (averaged over the cycle).

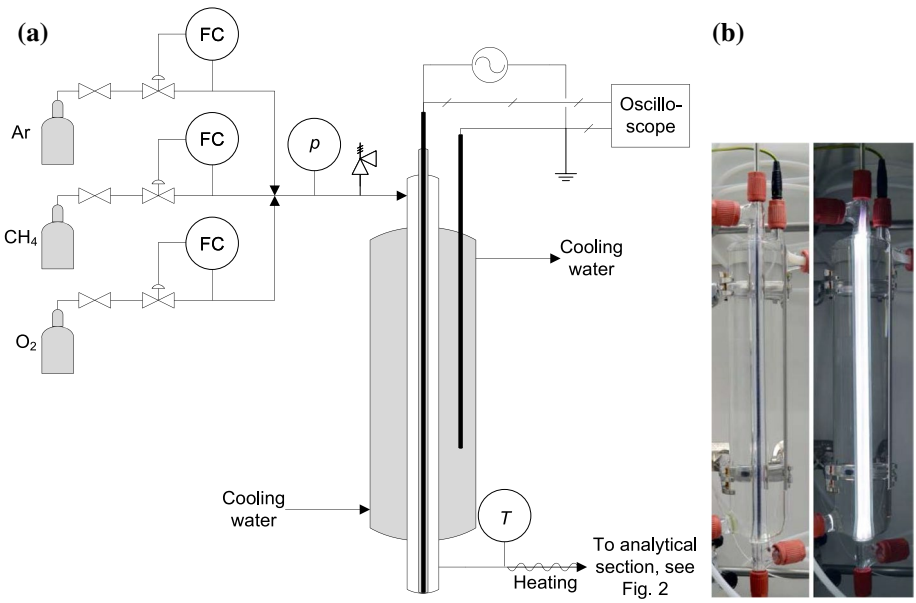

Fig. 1 **a** Cold plasma reactor with mass flow controllers (FC) for argon (Ar), methane (CH_4), and oxygen (O_2), the connection of the electrodes to the electrical equipment, as well as pressure p and temperature T measurement in the periphery. **b** Photographs of the cold plasma reactor during operation (left: daylight, right: dimmed light in laboratory)

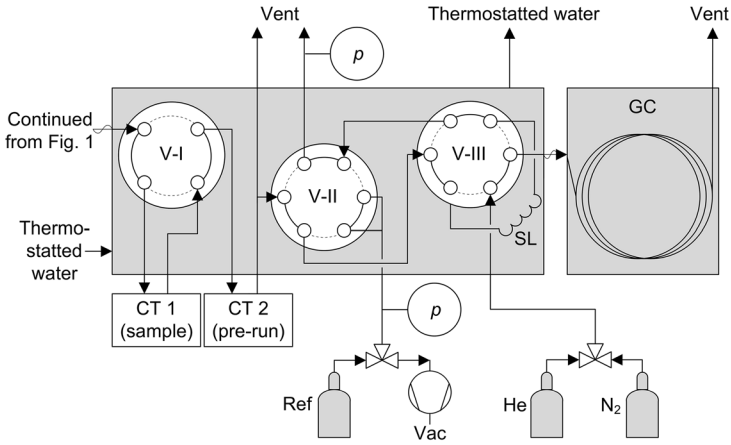

Fig. 2 Analytical system consisting of a temperature-controlled sampling unit with three multi-way valves, V-I to V-III. The valves provide connections to two cold traps (CT) and to a sample loop (SL) for the gas chromatographic analysis (GC). The sample loop can also be evacuated (Vac) or filled with an external reference gas (Ref). The GC can be operated with two carrier gases, helium (He) and nitrogen (N_2).

The instantaneous current $i(t)$ between the electrodes was measured with a current probe from Pearson Electronics (Model 6585). Both signals, $u(t)$ and $i(t)$, were recorded with a digital storage oscilloscope from Tektronix (TBS2104) with a sample interval of $8{\cdot}10^{-9}$ s. The effective power P fed to the reactor is calculated from Eq. (1)

$$P = \frac{1}{t_p} \int_{t=0}^{t_p} u(t)\, i(t)\, \mathrm{d}t \tag{1}$$

where t_p is the duration of one period. This method to calculate the power yields results which are equivalent to those from the Lissajous method and was recommended for plasma applications by Holub [51].

Table 1 provides information on the chemicals that were used in the experiments. All chemicals were used without further purification. The feed of the cold plasma reactor consisted of a mixture of Ar, CH_4, and O_2. The three gases were supplied from high-pressure cylinders equipped with pressure-reducing valves, which were set to pressures slightly above 1 bar. For monitoring and safety purposes, a pressure gauge (WIKA P-30) and a pressure relief valve were installed in the feed line of the plasma reactor. For analytical purposes, two pressure gauges (WIKA P-30 and MKS 690A13TRA) were installed in the analytical section, cf. Fig. 2. The uncertainty of the pressure measurement is 0.5 mbar for all gauges. The readings of the WIKA instruments were recorded with the WIKA Easy-Com 2011 software and noted manually for the MKS instrument. The flow rates of the three gases were controlled individually by three mass flow controllers from Bronkhorst (EL-FLOW Prestige). Additionally, the mass flow controllers measured and recorded the inlet temperature of the feed gases. The relative uncertainty of the mass flow measurement was 0.4%. The outlet temperature of the product stream was measured with a resistance thermometer from Temperatur Messelemente Hettstedt GmbH (Pt100). The readings of the thermometer and the Bronkhorst instruments were recorded using LabVIEW 2013. An electrical heating tape was installed around the line at the outlet of the reactor (cf. Fig. 1 panel a)), as condensation was detected there. The inlet and outlet temperatures

Table 1 Overview of the chemicals that were used in the experiments

Chemical	Supplier	Purity / g g^{-1}
Argon	Air Liquide	0.99999
Methane	Air Liquide	0.99500
Oxygen	Air Liquide	0.99998
Carbon dioxide	Air Liquide	0.99995
Helium	Air Liquide	0.99999
Hydrogen	Air Liquide	0.99999
Nitrogen	Air Liquide	0.99990
1,4-dioxane	Sigma-Aldrich	0.99900
Reference gas mixture[a]	Linde	0.99900

[a]0.76 mol mol^{-1} carbon monoxide, 0.19 mol mol^{-1} ethane, 0.05 mol mol^{-1} ethene

were averaged over the duration of each experiment. We specify the uncertainty of these average values as the uncertainty of the measurement including the standard deviation of the temperature fluctuations over the course of the experimental duration. The uncertainty of the average temperature at the reactor inlet is 1 K. Since the outlet temperature was additionally influenced by the following heating, the uncertainty of its mean value is 2 K. The cooling water for the thermostatization jacket was taken from a central supply line with an inlet temperature of about 291 K. A part of the analytical section, containing three main valves and a sample loop (cf. Fig. 2), was thermostatted to 313 K using a thermostat from Julabo (F25) with water as medium.

The volumetric feed flow rate was calculated from the mass flow rates and the results for the feed temperature and pressure using the ideal gas law. The residence time τ was calculated from the active reactor volume V (the volume that was illuminated) and the volumetric feed flow rate $\dot{V}^0$

$$\tau = \frac{V}{\dot{V}^0} \tag{2}$$

The specific energy input *SEI* was calculated by normalizing the power by the volumetric feed flow rate, as given by Eq. (3).

$$SEI = \frac{P}{\dot{V}^0} \tag{3}$$

In the analytical section, the product stream was split into a condensable fraction in a cold trap for offline analysis and into the remaining gaseous fraction that was analyzed at-line. Furthermore, the analytical section was equipped such that it can be evacuated, purged, and connected to a calibration gas supply. To achieve this, several valves were installed as shown in Fig. 2. V-I was a 4-way, 2-position valve from Swagelok (SS-45YF4); V-II and V-III were 6-way, 2-position valves from VICI (DC6WE). There are two cold traps, so that CT 1 was used for the *sampling* and CT 2 was used in the *pre-run* mode. The cold traps were made of glass and were operated at 195 K with a mixture of solid carbon dioxide and isopropanol. The valve position depicted in Fig. 2 is the one in which the sample is collected in CT 1 and the gaseous fraction is led to the GC for analysis.

For the start-up of the plant, V-I was switched to the *pre-run* mode, so that the product stream only passed CT 2. The primary voltage was set to a target value and subsequently,

the frequency was reduced beginning from its maximum value until cold plasma was present in the reactor. During this start-up, the cold plasma was not homogeneous, but lightning-type fluctuating luminous effects were observed, accompanied occasionally by a loud sizzling noise. Once homogeneous plasma was obtained and the noise stopped, the electrical parameters were kept constant; then, a steady-state in the reactor is reached, which took only a few minutes. V-I was then switched to *sampling* mode and the product stream was led to CT 1. The gas fraction from the outlet of CT 1 was first led through CT 2 and then split up. A part was released, the other part was led to the sampling valve V-III, which was equipped with a 100 µl sample loop. By switching V-III, samples from the sample loop were injected to the GC. This procedure was repeated several time during one stationary run. V-II was installed to switch between experiment and calibration and was not used during an experiment.

In the experiments of the present work, the residence time τ was varied from 0.5 to 4.7 s and the primary voltage from 12 to 44 V. All experiments were conducted with a feed composition of 0.750 mol mol^{-1} Ar, 0.167 mol mol^{-1} CH_4, and 0.083 mol mol^{-1} O_2. This corresponds to a molar reactant ratio (CH_4:O_2) in the feed of 2:1, which is above the upper explosion limit. With this feed composition, the necessary frequency to ignite the cold plasma was in a range from 10 to 14 kHz. The resulting power *P* and the *SEI* were in a range from 16 to 33 W and from 0.3 to 6.0 J cm^{-3}, respectively. The duration of the runtime in steady-state was chosen such that enough liquid sample was accumulated for analysis (about 3 ml) and so that at least six GC measurements were carried out, i.e., three for each carrier gas. On average, the duration of a single experiment was five hours. Detailed information on the individual experiments conducted in the present work with corresponding process parameters, electrical parameters, and numerical data is given in Table S 1 and Table S 2 in the Supporting Information.

Analysis of the Product Stream

Overview

Cold trap 1 was sealed at the end of the experiment and the trapped solid material was allowed to melt overnight. The mass of the sample in the cold trap (hereafter referred to as CT sample) was determined by means of differential weighing of CT 1 before and after the experiment using a balance from Mettler Toledo (PR1203, accuracy 1 mg). The CT sample was analyzed with NMR spectroscopy and wet-chemistry methods, which provided the mass fractions of the different components. The obtained mass fractions in the CT sample, the total mass of the CT sample from differential weighing, and the sampling time were used to calculate the molar component flows of the analyzed components. Further, the GC analysis provided the molar fractions of the components in the gaseous fraction of the product stream. The obtained molar fractions and the known molar flow of Ar were then used to calculate the molar component flows of the components analyzed by GC. Table 2 lists all components analyzed in the product stream. There, each component is provided with an abbreviation, which will be used hereafter for the sake of clarity.

The CT sample contains components that are reactive at ambient conditions also when they are not exposed to cold plasma. We only mention the classes of reactions here that have consequences for our work: with H_2O, FA reacts to MG and with alcohols, FA reacts to hemiformals [50]. Both these products can react further with FA yielding oligomers

Table 2 Overview on components of the product stream that were analyzed

Component	Abbrevia	Part	Analysis method
Acetic acid	HAc	CT	NMR
Acetone	Ace	CT	NMR
Argon	Ar	Gas	GC
Carbon dioxide	$CO_{2,liq}$	CT	NMR
	CO_2	Gas	GC
Carbon monoxide	CO	Gas	GC
Ethane	C_2H_6	Gas	GC
Ethanol	EtOH	CT	NMR
Ethene	C_2H_4	Gas	GC
Ethylene glycol	EG	CT	NMR
Formaldehyde	FA	CT	Sodium sulfite titration
Formic acid	FAc	CT	NMR
Hydrogen	H_2	Gas	GC
Hemiformal	HF	CT	Sodium sulfite titration and NMR
Hemiformal hydroperoxide	HFO	CT	Sodium sulfite titration and NMR
Methane	CH_4	Gas	GC
Methanol	MeOH	CT	NMR
Methyl acetate	MeAc	CT	NMR
Methyl formate	MeFo	CT	NMR
Methyl hydroperoxide	MeOOH	CT	NMR
Methylene glycol	MG	CT	Sodium sulfite titration and NMR
Oxygen	O_2	Gas	GC
Water	H_2O	CT	Karl Fischer titration

The table also lists whether the component was found in the cold trap (CT) or in the gaseous fraction after the cold trap (Gas)

(polyoxymethylene glycols and polyoxymethylene hemiformals in the case of MeOH as alcohol).

The titration methods we have used break up the reaction products, yielding what we call overall concentrations. In contrast, NMR analysis yields true concentrations, i.e., also information on the reaction products. The reactions of FA that are relevant for the present work are:

$$\mathrm{FA} + \mathrm{H_2O} \rightleftharpoons \mathrm{MG} \tag{I}$$

$$\mathrm{FA} + \mathrm{MeOH} \rightleftharpoons \mathrm{HF} \tag{II}$$

$$\mathrm{FA} + \mathrm{MeOOH} \rightleftharpoons \mathrm{HFO} \tag{III}$$

Formaldehyde oligomers were only detected in very small amounts and not quantified. It makes no sense to quantify MG, HF, and HFO individually in the CT sample as the species distribution in formaldehyde containing mixtures changes completely upon condensation. In particular, it is known that most of the FA is present as the monomer in the gas phase, whereas in the liquid phase, the concentration of monomeric FA is very low [45, 47, 48, 52–54]—so low that it could not be detected here. Hence, we ignore Reactions (I)–(III)

and instead directly report the overall concentrations that are obtained from the sodium sulfite titration for FA and from the Karl Fischer titration for H_2O. Similar to Reactions (I) – (III), reactions also occur with other aldehydes [55, 56]. For instance, acetaldehyde has been detected in the condensate of cold plasma oxidation of CH_4 by Larkin et al. [19, 20] and Goujard et al. [25], but reaction products of acetaldehyde with H_2O or alcohols were not found in this work.

Regarding the other products, we remark the following: Interestingly, CO_2 was only found in its molecular form and not as bicarbonate, as it might have been expected since the samples contain water. The reason is that the sample contains many acids, which leads to low pH values (about pH 2), which, in turn, favors the presence of monomeric CO_2. Furthermore, alcohols and acids can undergo esterification reactions [57–61]. The compounds involved in the esterification reactions could also have been formed in the gas phase. Therefore, esters were accounted for explicitly. The two esters that were quantified are MeAc and MeFo.

Although H_2O has been reported as a product of the partial oxidation of CH_4 with O_2, to the best of our knowledge, we are the first to quantify its amount. In the literature, the selectivity to H_2O is calculated—if at all—only from mass balance. MeOOH has been quantified for only one experiment by Goujard et al. [25] so far, who used ^{1}H NMR spectroscopy. As a result from structure elucidation, we have also assigned its hemiformal, HFO. In the present work, only HF and HFO were quantified by NMR spectroscopy, to account for their amount in the overall amount of MeOH and MeOOH, respectively. Further, we have detected and quantified MeAc and EG in the CT sample. The occurrence of neither of the components has been reported previously, not even qualitatively. Finally, we were able to identify and quantify additional components as products in the CT sample, namely MeFo, HAc, EtOH, and Ace. Although these products of cold plasma oxidation of CH_4 with O_2 have been reported previously (MeFo [17–20], HAc [27], EtOH [16, 27], Ace [27]), little quantitative data were available.

Wet-Chemistry

The mass fraction of H_2O in the CT sample was measured with the Karl Fischer titration method. The mass fraction of FA in the CT sample was measured with the sodium sulfite titration method with hydrochloric acid as titer [62]. Both wet-chemistry methods used in the present work directly provide the overall mass fractions [45, 47, 49, 62–65]. The uncertainties of the quantitative results from wet-chemistry are 0.01 g g^{-1} for the mass fraction of H_2O and 0.02 g g^{-1} for the mass fraction of FA. They were specified from the average deviation from repeated measurements including the weighing error.

NMR Spectroscopy

As the total number of moles in the CT sample was unknown, an internal standard, 1,4-dioxane (Diox), was used for calibration. The amount of Diox added to the sample was chosen such that the mass fraction of Diox in the resulting mixture was about 0.05 g g^{-1}. An analytical balance from Mettler Toledo (AG204 Delta Range, accuracy 0.1 mg) was used for preparation. Then, the sample was transferred to a 5 mm NMR tube and analyzed in a 400 MHz NMR spectrometer from Bruker (magnet: Ascend 400, console: Avance 3 HD 400, Double Resonance Broad Band Probe).

For the qualitative evaluation, a structure elucidation was carried out by combining information, such as the chemical shift and multiplicity of peaks, from one- and two-dimensional NMR techniques. In total, six types of NMR spectra were recorded: ^{1}H; ^{13}C inverse-gated ^{1}H-decoupled (hereafter referred to as ^{13}C); ^{13}C DEPT-135; ^{13}C without ^{1}H decoupling; ^{1}H,^{13}C HSQC; and ^{1}H,^{13}C HMBC. Figures 3 and 4 show the ^{1}H and ^{13}C NMR spectra of the CT sample gathered in one exemplary experiment at $SEI = 1.2$ J cm^{-3} (experiment 8, cf. Table S 1 in the Supporting Information) and Table 3 gives an overview of all assigned components and the corresponding peak labels. For some peaks in the ^{1}H NMR spectrum, also the ^{13}C satellites are visible, which are labeled with an asterisk (*) below the baseline. Peaks labeled with a question mark (?) have not been assigned. The remaining four types of acquired NMR spectra, i.e., ^{13}C without ^{1}H-decoupling; ^{13}C DEPT-135;

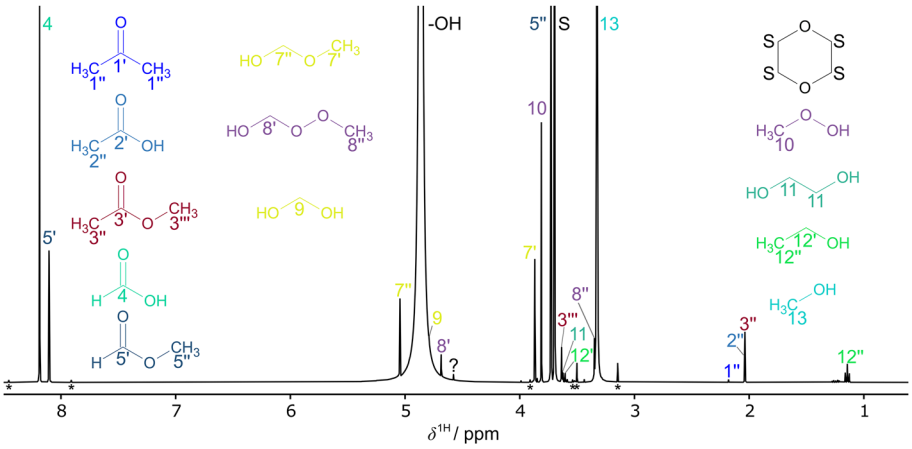

Fig. 3 ^{1}H NMR spectrum of the CT sample of experiment 8, the full intensities of some peaks are truncated for better visibility

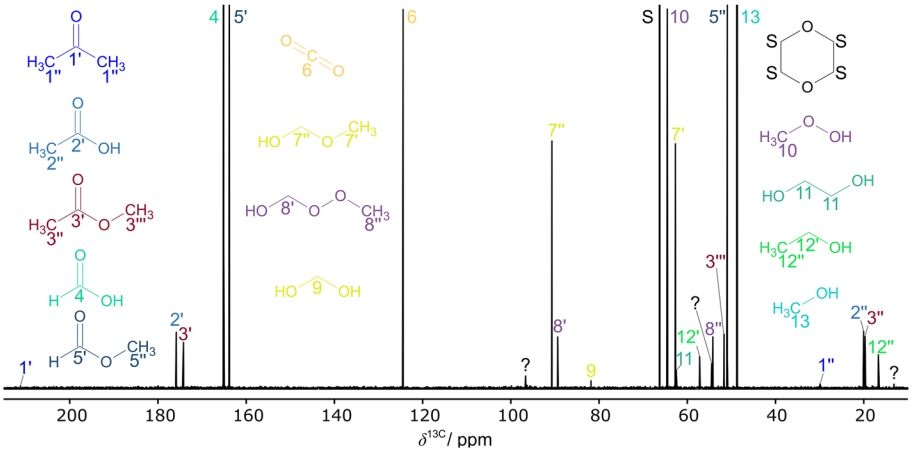

Fig. 4 ^{13}C NMR spectrum of the CT sample of experiment 8, the full intensities of some peaks are truncated for better visibility

Table 3 Peak assignment in the ^{1}H and ^{13}C NMR spectra obtained from the analysis of the CT sample.

Label	Component	Chemical formula	δ^{1H} / ppm	δ^{13C} / ppm
1'	Ace	$(CH_3)_2$**C**O		211.17
2'	HAc	CH_3**C**OOH		175.85
3'	MeAc	CH_3**C**OOCH_3		174.20
4	FAc	**H**COOH	8.19	165.10
5'	MeFo	**H**COOCH_3	8.10	163.82
6	$CO_{2,liq}$	**C**O_2		124.43
7''	HF	HO(**CH_2**O)CH_3	5.04	90.70
8'	HFO	HO(**CH_2**O)OCH_3	4.68	89.38
9	MG	HO(**CH_2**O)H	4.79	81.85
S	Internal standard Diox	**C_4H_8**O_2	3.70	66.30
10	MeOOH	**CH_3**OOH	3.81	64.54
7'	HF	HO(CH_2O)**CH_3**	3.87	62.70
11	EG	HO(**CH_2**)$_2$OH	3.63	62.52
12'	EtOH	CH_3**CH_2**OH	3.61	57.20
8''	HFO	HO(CH_2O)O**CH_3**	3.35	54.20
3'''	MeAc	CH_3COO**CH_3**	3.64	51.67
5''	MeFo	HCOO**CH_3**	3.73	50.93
13	MeOH	**CH_3**OH	3.33	48.72
1''	Ace	(**CH_3**)$_2$CO	2.18	29.86
2''	HAc	**CH_3**COOH	2.04	20.05
3''	MeAc	**CH_3**COOCH_3	2.04	19.70
12''	EtOH	**CH_3**CH_2OH	1.14	16.70
-OH	H_2O, hydroxyl groups	H_2O, –OH	4.86	

The bold font in the chemical formula indicates the functional group corresponding to the peak. The values of the shifts are those for the CT sample of experiment 8 at $SEI = 1.2$ J cm^{-3}.

^{1}H,^{13}C HSQC; and ^{1}H,^{13}C HMBC as well as further details on the structure elucidation are presented in the Supporting Information. Also, ^{1}H and ^{13}C NMR spectra of CT samples from two additional experiments at 0.4 and 6.0 J cm^{-3} are provided there. From the structure elucidation, we were able to assign 14 individual components. Among them, MG, HF, and HFO stem from the reactions of FA with H_2O, MeOH, and MeOOH (cf. Sect. "Overview", for more information on NMR spectroscopic analysis of formaldehyde-containing samples, see [45, 46, 49, 52, 66]).

For the quantitative evaluation, ^{1}H and ^{13}C NMR spectra were acquired at 303 K. The phase and baseline corrections were performed by using automatic routines from MestReNova (version 14.2.2). The full set of acquisition and processing parameters is listed in Table S 3 in the Supporting Information. The mass fractions of the components in the NMR sample were determined according to Eq. (4).

$$x_i^{(m),NMR} = \zeta_i x_{Diox}^{(m),NMR} \cdot \frac{M_i}{M_{Diox}} \tag{4}$$

where ζ_i is the molar ratio of component i to the internal standard and M_i is the molar mass of component i. The molar ratio ζ_i was calculated from the peak areas A_i^{NMR} accounting for the corresponding number of atoms N_i as indicated in Eq. (5).

$$\zeta_i = \frac{A_i^{\mathrm{NMR}}}{A_{\mathrm{Diox}}^{\mathrm{NMR}}} \cdot \frac{N_{\mathrm{Diox}}}{N_i} \tag{5}$$

The peak areas A_i^{NMR} were determined for peaks that were available for direct integration, i.e., where no overlapping with other peaks occurred. In general, peaks in ^{1}H NMR spectra show more overlap than peaks in ^{13}C NMR spectra due to the relatively high exchange rate of H atoms, especially those of the hydroxyl (-OH) groups, in contrast to C atoms. Hence, most of the components were quantified with ^{13}C NMR spectroscopy only, which was possible as quantitative NMR techniques were used.

For components for which more than one peak was available for direct integration, both peaks were used, and the obtained molar ratios were averaged. In Eqs. (4)–(5) i refers to either of the components Ace, $CO_{2,\mathrm{liq}}$, EG, EtOH, FAc, HAc, MeOH (incl. HF), MeOOH (incl. HFO), MeAc, and MeFo. The uncertainties of the mass fractions of the components obtained from quantitative NMR results are derived from the deviations between the results from ^{1}H and ^{13}C NMR spectra including the weighing error and are 0.01 g g^{-1}.

Gas Chromatography

The gaseous fraction of the product stream was analyzed at-line in a GC equipped with a thermal conductivity detector and a dual column from Agilent (GC: Series 6890, column: CP7430 comprised of PoraBOND Q and Molsieve 5 Å). Two different carrier gases, helium (He) and nitrogen (N_2), were used in all experiments, except for the experiments 1–7 (cf. Table S 1 in the Supporting Information), where only He was available. The two carrier gases were applied subsequently.

In the GC analysis, five products: CO, CO_2, C_2H_6, C_2H_4, and H_2, as well as the educts CH_4 and O_2, and the inert gas Ar were quantified. The assignment of retention times was done using reference components. In some experiments, a slight elevation of the baseline was detected in the chromatogram, which is probably caused by traces of the highly reactive ozone. This was verified by operating the DBD cold plasma reactor with only O_2 and Ar, which led to the same baseline elevation. We assume that ozone damages and reacts with the stationary phase of the column and, thus, does not elute giving a well-defined retention time but rather a broad baseline elevation.

For the quantitative evaluation, a calibration using reference gases was carried out in which the calibration factors k_i were determined by linear regression of known pairs of partial pressure p_i and area A_i^{GC} in the chromatogram. The accuracy of the GC analysis depends strongly on the uncertainty of the calibration factor. Where more than one signal was obtained for the same component for both carrier gases, the one with the higher calibration accuracy was used.

The areas from the chromatograms and determined calibration factors k_i are used to calculate the partial pressure p_i of the components in the gaseous fraction of the product stream as in Eq. (6).

$$p_i = k_i A_i^{\mathrm{GC}} \tag{6}$$

In Eq. (6), i refers to either of the components Ar, CH_4, O_2, CO_2, CO, H_2, C_2H_6, and C_2H_4. Each time V-III was switched to *injection* mode, the in-line pressure p (cf. Fig. 2) was recorded. Assuming a mixture of ideal gases, the mole fractions x_i in the gaseous fraction of the product stream can be calculated according to Eq. (7)

$$x_i = \frac{p_i}{p} \tag{7}$$

where p_i refers to the partial pressure of either of the components Ar, CH_4, O_2, CO_2, CO, H_2, C_2H_6, and C_2H_4. For each experiment, at least three chromatograms were recorded for each carrier gas during the steady-state operation. The resulting values for the mole fractions were then averaged for each component. The only exception is the noble gas Ar, which is not converted in the cold plasma reactions and for which we have neglected the solubility in the CT sample. Hence, Ar was used as an internal reference gas with a known molar flow, allowing for the calculation of the total molar flow of the gaseous fraction of the product stream. Two typical chromatograms—one for each carrier gas—with the retention times and information on GC acquisition parameters as well as the calibration factors and individual standard uncertainties are compiled in the Supporting Information.

Conversions and Selectivities

The conversion X_j is defined as given in Eq. (8)

$$X_j = \frac{\dot{n}_j^0 - \dot{n}_j}{\dot{n}_j^0} \tag{8}$$

where j refers to either of the reactants CH_4 or O_2, $\dot{n}_j^0$ refers to the molar flow at the inlet, and $\dot{n}_j$ refers to the molar flow at the outlet of the reactor.

The selectivity to the product components was calculated accounting for the number of C atoms in the product component (hereafter referred to as C-selectivity). The C-selectivity to 14 product components, i.e., Ace, CO, CO_2, C_2H_6, C_2H_4, EG, EtOH, FA, FAc, HAc, MeAc, MeFo, MeOH, and MeOOH was calculated as defined in Eq. (9)

$$S_{i,\mathrm{C}} = \frac{\dot{n}_i}{\dot{n}_{\mathrm{CH_4}}^0 - \dot{n}_{\mathrm{CH_4}}} \cdot \frac{1}{\nu_{i,\mathrm{C}}} \tag{9}$$

where $\nu_{i,\mathrm{C}}$ is the number of C atoms in component i and $\dot{n}_j$ refers to the molar flow of the product component at the outlet of the reactor. For CO_2, the sum of the molar component flows of the CT sample and the gaseous fraction was used. The selectivity to the product components without any C atoms was calculated accounting for the number of H atoms in CH_4 and in the product component, respectively (hereafter referred to as H-selectivity). The H-selectivity to the two product components H_2O and H_2 was calculated as defined in Eq. (10)

$$S_{i,\mathrm{H}} = \frac{\dot{n}_i}{\dot{n}_{\mathrm{CH_4}}^0 - \dot{n}_{\mathrm{CH_4}}} \cdot \frac{4}{\nu_{i,\mathrm{H}}} \tag{10}$$

where $\nu_{i,\mathrm{H}}$ is the number of H atoms in component i.

The uncertainties of the conversions and selectivities were calculated individually for each experiment from error propagation including all analytical uncertainties as stated above.

Results and Discussion

General Remarks

As the individual results scatter quite strongly, it is hard to discern trends from corresponding plots. Therefore, for the representation in Figs. 5, 6, and 7, the results from experiments with approximately the same *SEI* (interval width 0.3 J cm^{-3}) were used to obtain a single averaged value, which is plotted together with the standard deviation of the results from the average. Where there was only a single value in the interval, the error bar was obtained from the average of the standard deviations of the other data points. Additionally, the results from linear fits through the data points are shown. The full set of numerical results and plots of the individual data points are given in the Supporting Information.

The electrical energy required to produce one mole of product is in a range from 0.5 to 1.0 kWh mol^{-1}. The products are defined hereby as all components excluding the non-converted reactants as well as H_2O and CO_2.

Conversions

Figure 5 shows the results for the conversions X_j of CH_4 and O_2 as a function of the *SEI*. While the conversion of O_2 covers basically the entire range up to full conversion, the maximal conversion of CH_4 is about 0.32, which is a consequence of the excess of CH_4 over O_2 in the feed. The conversion of O_2 increases linearly with increasing *SEI*. A similar trend is observed for the conversion of CH_4. In the present work, the variation of *SEI* was obtained by varying the power *P* and the residence time τ, as the *SEI* combines both variables into a single variable (cf. Eq. (3)).

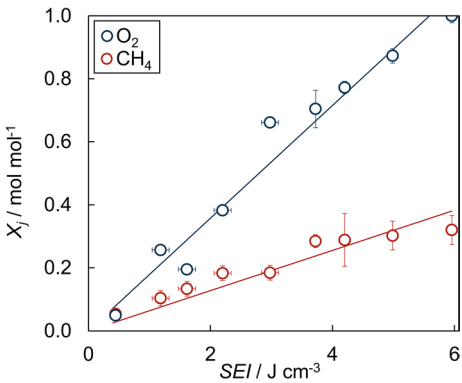

Fig. 5 Conversions of CH_4 and O_2

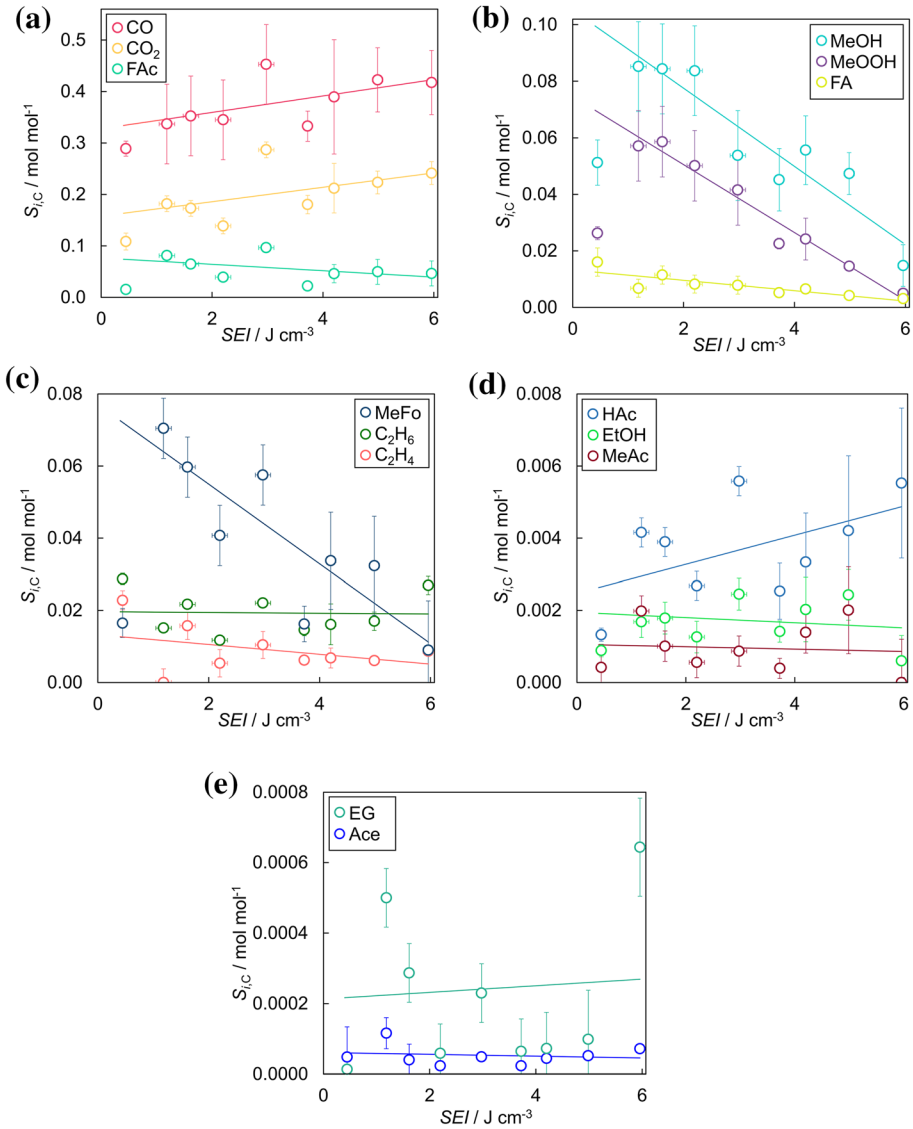

Fig. 6 C-selectivities to **a** CO, CO_2, FAc; **b** MeOH, MeOOH, FA; **c** MeFo, C_2H_6, C_2H_4; **d** HAc, EtOH, and MeAc; and **e** EG and Ace

Selectivities

Figure 6 panels a–e show the C-selectivities to all carbon-containing products that were quantified in this work. In comparing the results from the different panels in Fig. 6, the different scales for the selectivity should be considered. In some cases, the value of the selectivity obtained at the smallest *SEI* deviates strongly from the general trend, such that it was not included in the data base for the fit. At the smallest *SEI,* the residence

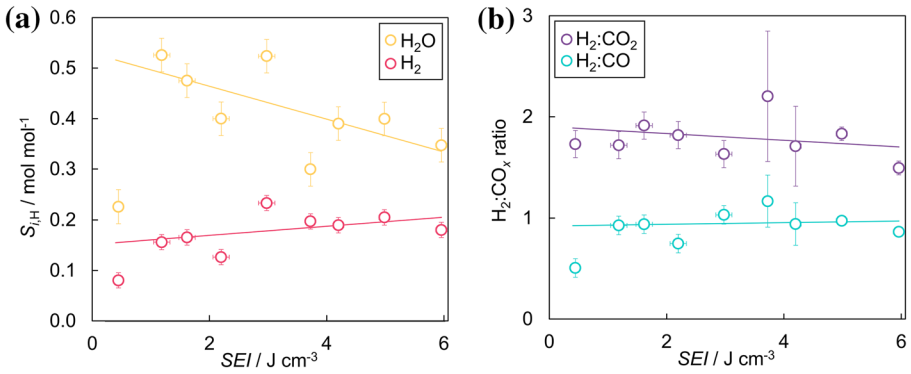

Fig. 7 **a** H-selectivities to H_2O and H_2 and **b** molar ratio of (H_2:CO_2) and (H_2:CO)

time of all experiments in this interval is 0.5 s, which is the shortest of all, and the average temperature increase between the reactor inlet and outlet is about 20 K, whereas it is only about 5 K in all other experiments. The deviations from the general trend that were observed for the selectivity along with a higher temperature increase in the reactor could origin from exothermic reactions taking place that have a significantly higher absolute reaction enthalpy. Results from an element balance also indicate that the highest number of undetected elements is present at the smallest *SEI*. Taking the measurement uncertainties into account, the element balances are closed for all experiments and all three elements, i.e., C, H, and O atoms. More information on the temperatures and the element balances are given in the Supporting Information.

Although the C-selectivities to a few components scatter significantly, still trends can be discerned: the C-selectivities to CO and CO_2 increase with increasing *SEI* and the inverse tendency seems to hold for the C-selectivities to FAc, MeOH, MeOOH, FA, and MeFo. For the C-selectivities to C_2H_6, C_2H_4, HAc, EtOH, MeAc, EG, and Ace no clear trend is discernable. In general, the C-selectivities to many oxidized products present in the CT sample (FAc, MeOH, MeOOH, FA, and MeFo) decrease with increasing *SEI*, while the selectivities to oxidized products present in the remaining gaseous stream, i.e., CO and CO_2 increase with increasing *SEI*.

Figure 7 panel a shows the H-selectivities to H_2O and H_2. Again, the results found for the smallest *SEI* deviate strongly from the general trend. Furthermore, the amount of H_2 found for the lowest *SEI* was below the limit of detection in most cases. For *SEI* above about 1 J cm^{-3}, the H-selectivity to H_2O decreases with increasing *SEI*, while the H-selectivity to H_2 increases.

Obviously, the C-selectivities and the H-selectivities are directly coupled. As an example, we show molar ratios of (H_2:CO_2) and (H_2:CO) in the product stream as a function of *SEI* in Fig. 7 panel b. As mentioned above, at the lowest *SEI,* the concentration of H_2 exceeded the limit of detection only in one experiment. For *SEI* above 1 J cm^{-3}, the molar ratio of (H_2:CO) was about 0.95 ± 0.11, while the molar ratio of (H_2:CO_2) was about 1.80 ± 0.20. These almost constant values of the molar ratios are the result of the same trends of the conversions to H_2 on the one side and CO and CO_2 on the other side, which both rise with *SEI* (cf. Figure 7 panel a and Fig. 6 panel a).

The trends for the selectivities as a function of residence time, observed in the experiments of the present work, are compared in the following to trends observed in previous experimental

studies from the literature of the partial oxidation of CH_4 with O_2 in non-catalyzed DBD cold plasma reactors. Also, predictions of these trends from reaction kinetic models are included in this qualitative comparison.

The experimental results of Yi et al. [40] for CO, CO_2, MeOH, FAc, and FA, and of Larkin et al. [18] for H_2 confirm the trends found in the present work. The trends observed by Larkin et al. [18] for MeFo and C_2H_6 and by Bhatnagar and Mallison [16] for EtOH, do not agree with those from our study. To the best of our knowledge, for all other product components discussed in the present work, i.e., MeOOH, C_2H_4, HAc, MeAc, EG, Ace, and H_2O, no experimental data on the dependence of the selectivity on the residence time is available.

De Bie et al. [41] have recently published a detailed reaction kinetic model of the partial oxidation of CH_4 with O_2 in DBD cold plasma reactors. For CO, CO_2, and H_2, their model predicts the same trends for the selectivity as observed in the present work, while for MeOH, MeOOH, FA, and H_2O the opposite trends were found. Furthermore, EtOH as well as hydrocarbons are included in the model of De Bie et al. [41], however, they report that these components are only present in trace amounts in the product in experiments with partial conversion of oxygen (as they were carried out in the present work) and no statement on the influence of the residence time is made. In the experiments of the present work, EtOH is a minor component, as predicted by the model of De Bie et al. [41], however, substantial amounts of hydrocarbons were found. All other products, for which experimental data are provided in the present work, i.e., FAc, MeFo, HAc, MeAc, EG, and Ace, were not included in the model of De Bie et al. [41].

Besides the experimental data discussed above, Yi et al. [40] report also results from reaction kinetic modeling. For CO, CO_2, and MeOH, they found similar trends as those observed in the present work, while for FAc the opposite trend was found. HAc as well as EtOH were predicted to be only present in trace amounts, which is confirmed by the results from the present study.

This short comparison shows that there is still much work to do on the way to predictive reaction kinetic modeling of the partial oxidation of CH_4 with O_2 in DBD cold plasma reactors. The qualitative trends for the selectivities to CO and CO_2 are predicted correctly by the discussed models from the literature, but for most of the other components, open questions remain: there are contradictions between the predictions of different models, but also contradictions between experimental data from different sources. Furthermore, the available models do not cover many of the components for which we have provided data now.

These open questions are not astonishing; they are a consequence of the complexity of a reaction network that is triggered by the cold plasma and the lack of data which is needed to test and parametrize the corresponding complex models. The present work provides both qualitative and quantitative experimental data which are needed for this purpose.

Conclusions

In the present work, a detailed analysis of the product spectrum, obtained during the partial oxidation of methane (CH_4) with oxygen (O_2) in a dielectric barrier discharge (DBD) cold plasma reactor, was performed in a series of 23 experiments. The reactor was operated near ambient conditions and argon was used as inert gas. The feed composition was the same in all experiments: the molar reactant ratio (CH_4:O_2) was 2:1, the argon mole fraction was 0.75 mol mol^{-1}.

The influence of the variation of the electrical power P and the volumetric feed flow rate $\dot{V}^0$ (i.e., the residence time τ in the reactor) can be described well by lumping both factors into the specific energy input $SEI = P/\dot{V}^0$.

A comprehensive qualitative and quantitative analysis of the product spectrum as well as unconverted feed components was conducted by a combination of NMR spectroscopy, wet-chemistry methods, and gas chromatography. All in all, quantitative results are reported for 16 components, more than in any previous study of partial oxidation of CH_4 with O_2 in cold plasma.

The variation of the *SEI* was performed in the range from 0.3 to 6.0 J cm^{-3}, where a roughly linear influence of the *SEI* on the conversions of CH_4 and O_2 was found. In contrast, the influence of the *SEI* on the selectivities to the different products depends strongly on the products: the selectivities to carbon monoxide, carbon dioxide, and hydrogen were found to increase with increasing *SEI*, while those for the products formic acid, methanol, methyl hydroperoxide, formaldehyde, methyl formate, and water decreased with increasing *SEI*. For the selectivities to ethane, ethene, acetic acid, ethanol, methyl acetate, ethylene glycol, and acetone, no clear trend was found. The molar ratios of hydrogen to carbon monoxide and to carbon dioxide were found to be independent of the *SEI* and were $(H_2{:}CO) = 1$ and $(H_2{:}CO_2) = 1.8$.

Cold plasma enables new reaction routes at mild conditions, which is boon and bane at the same time. The new options are highly interesting, but they come at the price of a broad product spectrum. Learning how we can influence that product spectrum is worthwhile and should not only rely on empirical studies as the one we have carried out here. The key is to understand the complex reaction network that is triggered by the cold plasma. Developing reaction kinetic models to describe this network and the influence of the different process parameters on it is a formidable task. Its success strongly depends on the availability of sufficiently large sets of meaningful experimental data. First steps on this way have already been taken in the literature but qualitative predictions from available models are still uncertain, whereas the ultimate goal would be quantitative predictions. The new experimental data provided in the present work are a valuable asset for the future work in this field.

Supplementary Information The online version contains supplementary material available at https://doi.org/10.1007/s11090-022-10308-5.

Funding Open Access funding enabled and organized by Projekt DEAL.

Declarations

Conflict of interest The authors have no relevant financial or non-financial interests to disclose.

Open Access This article is licensed under a Creative Commons Attribution 4.0 International License, which permits use, sharing, adaptation, distribution and reproduction in any medium or format, as long as you give appropriate credit to the original author(s) and the source, provide a link to the Creative Commons licence, and indicate if changes were made. The images or other third party material in this article are included in the article's Creative Commons licence, unless indicated otherwise in a credit line to the material. If material is not included in the article's Creative Commons licence and your intended use is not permitted by statutory regulation or exceeds the permitted use, you will need to obtain permission directly from the copyright holder. To view a copy of this licence, visit http://creativecommons.org/licenses/by/4.0/.

References

1. Fridman A (2008) Plasma chemistry. Cambridge University Press, Cambridge
2. Kogelschatz U (2003) Dielectric-barrier discharges: their history, discharge physics, and industrial applications. Plasma Chem Plasma Process 23:1–46. https://doi.org/10.1023/A:1022470901385
3. Fridman A, Kennedy LA (2004) Plasma physics and engineering. CRC Press, Boca Raton
4. Eliasson B, Kogelschatz U (1991) Nonequilibrium volume plasma chemical processing. IEEE Trans Plasma Sci 19:1063–1077. https://doi.org/10.1109/27.125031
5. Bogaerts A, Neyts E, Gijbels R, van der Mullen J (2002) Gas discharge plasmas and their applications. Spectrochim Acta Part B At Spectrosc 57:609–658. https://doi.org/10.1016/S0584-8547(01)00406-2
6. Siemens W (1857) Ueber die elektrostatische Induction und die Verzögerung des Stroms in Flaschendrähten. Ann Phys Chem 178:66–122. https://doi.org/10.1002/andp.18571780905
7. Malik MA, Ghaffar A, Malik SA (2001) Water purification by electrical discharges. Plasma Sources Sci Technol 10:82–91. https://doi.org/10.1088/0963-0252/10/1/311
8. Nitsche T, Unger C, Weidner E (2018) Plasma catalytical reactors for atmospheric gas conversions. Chem Ing Tech 90:1453–1464. https://doi.org/10.1002/cite.201800024
9. Indarto A (2008) A review of direct methane conversion to methanol by dielectric barrier discharge. IEEE Trans Dielectr Electr Insul 15:1038–1043. https://doi.org/10.1109/TDEI.2008.4591225
10. Nozaki T, Ağıral A, Yuzawa S, Han Gardeniers JGE, Okazaki K (2011) A single step methane conversion into synthetic fuels using microplasma reactor. Chem Eng J 166:288–293. https://doi.org/10.1016/j.cej.2010.08.001
11. Suhr H (1983) Application of nonequilibrium plasmas in organic chemistry. Plasma Chem Plasma Process 3:1–61. https://doi.org/10.1007/BF00566027
12. Aerts R, Somers W, Bogaerts A (2015) Carbon dioxide splitting in a dielectric barrier discharge plasma: a combined experimental and computational study. Chemsuschem 8:702–716. https://doi.org/10.1002/cssc.201402818
13. Aghamir FM, Matin NS, Jalili AH, Esfarayeni MH, Khodagholi MA, Ahmadi R (2004) Conversion of methane to methanol in an ac dielectric barrier discharge. Plasma Sources Sci Technol 13:707–711. https://doi.org/10.1088/0963-0252/13/4/021
14. Thanyachotpaiboon K, Chavadej S, Caldwell TA, Lobban LL, Mallinson RG (1998) Conversion of methane to higher hydrocarbons in AC nonequilibrium plasmas. AIChE J 44:2252–2257. https://doi.org/10.1002/aic.690441014
15. Alvarez-Galvan MC, Mota N, Ojeda M, Rojas S, Navarro RM, Fierro JLG (2011) Direct methane conversion routes to chemicals and fuels. Catal Today 171:15–23. https://doi.org/10.1016/j.cattod.2011.02.028
16. Bhatnagar R, Mallinson RG (1995) Methane conversion in AC electric discharges at ambient conditions. Methane and alkane conversion chemistry. Springer, Boston, MA, pp 249–264
17. Larkin DW, Caldwell TA, Lobban LL, Mallinson RG (1998) Oxygen pathways and carbon dioxide utilization in methane partial oxidation in ambient temperature electric discharges. Energy Fuels 12:740–744. https://doi.org/10.1021/ef970217n
18. Larkin DW, Zhou L, Lobban LL, Mallinson RG (2001) Product selectivity control and organic oxygenate pathways from partial oxidation of methane in a silent electric discharge reactor. Ind Eng Chem Res 40:5496–5506. https://doi.org/10.1021/ie010298h
19. Larkin DW, Lobban LL, Mallinson RG (2001) The direct partial oxidation of methane to organic oxygenates using a dielectric barrier discharge reactor as a catalytic reactor analog. Catal Today 71:199–210. https://doi.org/10.1016/S0920-5861(01)00430-8
20. Larkin DW, Lobban LL, Mallinson RG (2001) Production of organic oxygenates in the partial oxidation of methane in a silent electric discharge reactor. Ind Eng Chem Res 40:1594–1601. https://doi.org/10.1021/ie000527k
21. Indarto A, Cho J-W, Lee H, Song HK, Palgunadi J (2006) Partial oxidation of methane with sol-gel Fe/Hf/YSZ catalyst in dielectric barrier discharge: catalyst activation by plasma. J Rare Earths 24:513–518. https://doi.org/10.1016/S1002-0721(06)60154-3
22. Indarto A, Yang DR, Palgunadi J, Choi J-W, Lee H, Song HK (2008) Partial oxidation of methane with Cu–Zn–Al catalyst in a dielectric barrier discharge. Chem Eng Process Process Intensif 47:780–786. https://doi.org/10.1016/j.cep.2006.12.015
23. Nozaki T, Hattori A, Okazaki K (2004) Partial oxidation of methane using a microscale non-equilibrium plasma reactor. Catal Today 98:607–616. https://doi.org/10.1016/j.cattod.2004.09.053
24. Ağıral A, Nozaki T, Nakase M, Yuzawa S, Okazaki K, Gardeniers JGE (2011) Gas-to-liquids process using multi-phase flow, non-thermal plasma microreactor. Chem Eng J 167:560–566. https://doi.org/10.1016/j.cej.2010.10.050

25. Goujard V, Nozaki T, Yuzawa S, Ağiral A, Okazaki K (2011) Plasma-assisted partial oxidation of methane at low temperatures: numerical analysis of gas-phase chemical mechanism. J Phys Appl Phys 44:274011. https://doi.org/10.1088/0022-3727/44/27/274011
26. Zhou J, Xu Y, Zhou X, Gong J, Yin Y, Zheng H, Guo H (2011) Direct oxidation of methane to hydrogen peroxide and organic oxygenates in a double dielectric plasma reactor. Chemsuschem 4:1095–1098. https://doi.org/10.1002/cssc.201100093
27. Chawdhury P, Wang Y, Ray D, Mathieu S, Wang N, Harding J, Bin F, Tu X, Subrahmanyam Ch (2021) A promising plasma-catalytic approach towards single-step methane conversion to oxygenates at room temperature. Appl Catal B Environ 284:119735. https://doi.org/10.1016/j.apcatb.2020.119735
28. Nair SA, Nozaki T, Okazaki K (2007) Methane oxidative conversion pathways in a dielectric barrier discharge reactor—Investigation of gas phase mechanism. Chem Eng J 132:85–95. https://doi.org/10.1016/j.cej.2007.01.022
29. Loenders B, Engelmann Y, Bogaerts A (2021) Plasma-catalytic partial oxidation of methane on Pt(111): a microkinetic study on the role of different plasma species. J Phys Chem C 125:2966–2983. https://doi.org/10.1021/acs.jpcc.0c09849
30. Nozaki T, Okazaki K (2012) Plasma enhanced C1-chemistry: towards greener methane conversion. Green Process Synth 1:517–523. https://doi.org/10.1515/gps-2012-0074
31. Wang B, Zhang X, Liu Y, Xu G (2009) Conversion of CH4, steam and O2 to syngas and hydrocarbons via dielectric barrier discharge. J Nat Gas Chem 18:94–97. https://doi.org/10.1016/S1003-9953(08)60089-4
32. Nozaki T, Abe S, Moriyama S, Kameshima S, Okazaki K, Goujard V, Ağıral A (2015) One step methane conversion to syngas by dielectric barrier discharge. Jpn J Appl Phys. https://doi.org/10.7567/JJAP.54.01AG01
33. Zou J-J, Zhang Y, Liu C-J, Li Y, Eliasson B (2003) Starch-enhanced synthesis of oxygenates from methane and carbon dioxide using dielectric-barrier discharges. Plasma Chem Plasma Process 23:69–82. https://doi.org/10.1023/A:1022416819132
34. Nozaki T, Goujard V, Yuzawa S, Moriyama S, Ağıral A, Okazaki K (2011) Selective conversion of methane to synthetic fuels using dielectric barrier discharge contacting liquid film. J Phys Appl Phys 44:274010. https://doi.org/10.1088/0022-3727/44/27/274010
35. Zhou LM, Xue B, Kogelschatz U, Eliasson B (1998) Partial oxidation of methane to methanol with oxygen or air in a nonequilibrium discharge plasma. Plasma Chem Plasma Process 18:375–393
36. Seyed Matin N, Savadkoohi HA, Feizabadi SY (2008) Methane conversion to C2 hydrocarbons using dielectric-barrier discharge reactor: effects of system variables. Plasma Chem Plasma Process 28:189–202. https://doi.org/10.1007/s11090-008-9123-5
37. Okumoto M, Mizuno A (2001) Conversion of methane for higher hydrocarbon fuel synthesis using pulsed discharge plasma method. Catal Today 71:211–217. https://doi.org/10.1016/S0920-5861(01)00431-X
38. Okumoto M, Kim HH, Takashima K, Katsura S, Mizuno A (2001) Reactivity of methane in nonthermal plasma in the presence of oxygen and inert gases at atmospheric pressure. IEEE Trans Ind Appl 37:1618–1624. https://doi.org/10.1109/28.968169
39. Pietruszka B, Heintze M (2004) Methane conversion at low temperature: the combined application of catalysis and non-equilibrium plasma. Catal Today 90:151–158. https://doi.org/10.1016/j.cattod.2004.04.021
40. Yi Y, Li S, Cui Z, Hao Y, Zhang Y, Wang L, Liu P, Tu X, Xu X, Guo H, Bogaerts A (2021) Selective oxidation of CH4 to CH3OH through plasma catalysis: insights from catalyst characterization and chemical kinetics modelling. Appl Catal B Environ 296:120384. https://doi.org/10.1016/j.apcatb.2021.120384
41. De Bie C, van Dijk J, Bogaerts A (2015) The dominant pathways for the conversion of methane into oxygenates and syngas in an atmospheric pressure dielectric barrier discharge. J Phys Chem C 119:22331–22350. https://doi.org/10.1021/acs.jpcc.5b06515
42. Snoeckx R, Ozkan A, Reniers F, Bogaerts A (2017) The quest for value-added products from carbon dioxide and water in a dielectric barrier discharge: a chemical kinetics study. Chemsuschem 10:409–424. https://doi.org/10.1002/cssc.201601234
43. Hong J, Prawer S, Murphy AB (2014) Production of ammonia by heterogeneous catalysis in a packed-bed dielectric-barrier discharge: influence of argon addition and voltage. IEEE Trans Plasma Sci 42:2. https://doi.org/10.1109/TPS.2014.2323077
44. Pinhao NR, Janeco A, Branco JB (2011) Influence of helium on the conversion of methane and carbon dioxide in a dielectric barrier discharge. Plasma Chem Plasma Process 31:427–439. https://doi.org/10.1007/s11090-011-9294-3
45. Kircher R, Schmitz N, Berje J, Münnemann K, Thiel WR, Burger J, Hasse H (2020) Generalized chemical equilibrium constant of formaldehyde oligomerization. Ind Eng Chem Res 59:11431–11440. https://doi.org/10.1021/acs.iecr.0c00974

46. Schmitz N, Homberg F, Berje J, Burger J, Hasse H (2015) Chemical equilibrium of the synthesis of poly(oxymethylene) dimethyl ethers from formaldehyde and methanol in aqueous solutions. Ind Eng Chem Res 54:6409–6417. https://doi.org/10.1021/acs.iecr.5b01148
47. Kuhnert C, Albert M, Breyer S, Hahnenstein I, Hasse H, Maurer G (2006) Phase equilibrium in formaldehyde containing multicomponent mixtures: experimental results for fluid phase equilibria of (formaldehyde + (water or methanol) + methylal)) and (formaldehyde + water + methanol + methylal) and comparison with predictions. Ind Eng Chem Res 45:5155–5164. https://doi.org/10.1021/ie060131u
48. Maiwald M, Fischer HH, Ott M, Peschla R, Kuhnert C, Kreiter CG, Maurer G, Hasse H (2003) Quantitative NMR spectroscopy of complex liquid mixtures: methods and results for chemical equilibria in formaldehyde−water−methanol at temperatures up to 383 K. Ind Eng Chem Res 42:259–266. https://doi.org/10.1021/ie0203072
49. Hahnenstein I, Hasse H, Kreiter CG, Maurer G (1994) 1H- and 13C-NMR-spectroscopic study of chemical equilibria in solutions of formaldehyde in water, deuterium oxide, and methanol. Ind Eng Chem Res 33:1022–1029. https://doi.org/10.1021/ie00028a033
50. Maurer G (1986) Vapor-liquid equilibrium of formaldehyde-and water-containing multicomponent mixtures. AIChE J 32:932–948. https://doi.org/10.1002/aic.690320604
51. Hołub M (2012) On the measurement of plasma power in atmospheric pressure DBD plasma reactors. Int J Appl Electromagn Mech 39:81–87. https://doi.org/10.3233/JAE-2012-1446
52. Dyga M, Keller A, Hasse H (2021) Vapor-liquid equilibria and chemical equilibria in the system (formaldehyde + water + isoprenol). Ind Eng Chem Res 60:4471–4483. https://doi.org/10.1021/acs.iecr.1c00168
53. Albert M, Hahnenstein I, Hasse H, Maurer G (2001) Vapor−liquid and liquid−liquid equilibria in binary and ternary mixtures of water, methanol, and methylal. J Chem Eng Data 46:897–903. https://doi.org/10.1021/je000352l
54. Albert M, Coto García B, Kuhnert C, Peschla R, Maurer G (2000) Vapor–liquid equilibrium of aqueous solutions of formaldehyde and methanol. AIChE J 46:1676–1687. https://doi.org/10.1002/aic.690460818
55. Scheithauer A, von Harbou E, Hasse H, Grützner T, Rijksen C, Zollinger D, Thiel WR (2015) ^{1}H- and ^{13}C-NMR spectroscopic study of chemical equilibria in the system acetaldehyde + water. AIChE J 61:177–187. https://doi.org/10.1002/aic.14623
56. Scheithauer A, Grützner T, Rijksen C, Zollinger D, von Harbou E, Thiel WR, Hasse H (2014) NMR spectroscopic study of the aldoxane formation in aqueous acetaldehyde solutions. Ind Eng Chem Res 53:8395–8403. https://doi.org/10.1021/ie5004043
57. von Harbou E, Behrens R, Berje J, Brächer A, Hasse H (2017) Studying fast reaction kinetics with online NMR spectroscopy. Chem Ing Tech 89:369–378. https://doi.org/10.1002/cite.201600068
58. Brächer A, Hoch S, Albert K, Kost HJ, Werner B, von Harbou E, Hasse H (2014) Thermostatted microreactor NMR probe head for monitoring fast reactions. J Magn Reson 242:155–161. https://doi.org/10.1016/j.jmr.2014.02.013
59. Brächer A, Behrens R, von Harbou E, Hasse H (2016) Application of a new micro-reactor 1 H NMR probe head for quantitative analysis of fast esterification reactions. Chem Eng J 306:413–421. https://doi.org/10.1016/j.cej.2016.07.045
60. Friebel A, von Harbou E, Münnemann K, Hasse H (2019) Reaction monitoring by benchtop NMR spectroscopy using a novel stationary flow reactor setup. Ind Eng Chem Res 58:18125–18133. https://doi.org/10.1021/acs.iecr.9b03048
61. Berje J, Burger J, Hasse H, Baldamus J (2017) NMR spectroscopic study of chemical equilibria in solutions of formaldehyde, water, and butynediol. AIChE J 63:4442–4450. https://doi.org/10.1002/aic.15788
62. Walker JF (1953) Formaldehyde, 2nd edn. Reinhold Publishing Corp, New York
63. Rivlin M, Eliav U, Navon G (2015) NMR studies of the equilibria and reaction rates in aqueous solutions of formaldehyde. J Phys Chem B 119:4479–4487. https://doi.org/10.1021/jp513020y
64. Hahnenstein I, Albert M, Hasse H, Kreiter CG, Maurer G (1995) NMR spectroscopic and densimetric study of reaction kinetics of formaldehyde polymer formation in water, deuterium oxide, and methanol. Ind Eng Chem Res 34:440–450. https://doi.org/10.1021/ie00041a003
65. Gaca KZ, Parkinson JA, Lue L, Sefcik J (2014) Equilibrium speciation in moderately concentrated formaldehyde–methanol–water solutions investigated using 13C and 1H nuclear magnetic resonance spectroscopy. Ind Eng Chem Res 53:9262–9271. https://doi.org/10.1021/ie403252x
66. Dyga M, Keller A, Hasse H (2021) 13C-NMR spectroscopic study of the kinetics of formaldehyde oligomerization reactions in the system (formaldehyde + water + isoprenol). Ind Eng Chem Res. https://doi.org/10.1021/acs.iecr.1c03911

Publisher's Note Springer Nature remains neutral with regard to jurisdictional claims in published maps and institutional affiliations.